Multifunctional Soft Transducer for Electrical and Optical Sensing Applied to Fatigue Crack Monitoring

HAN LIU, MATTHIAS KOLLOSCHE, SIMON LAFLAMME and DAVID R. CLARKE

ABSTRACT The timely discovery and monitoring of fatigue cracks on steel bridges is critical in ensuring structural safety and continuous operations. Existing sensing solutions, for example foil gauges, can be used to monitor known cracks, yet cannot be used for crack discovery because of their highly localized nature. A solution is the development and deployment of large-area electronics capable of detecting local states over large surfaces. Polymer-based nano-structured materials that respond to external impacts, such as mechanical strain, with color changing properties have attracted significant attention in structural health monitoring (SHM) community, because their passive optical/visual properties can be used to assist inspectors at quickly localizing new fatigue cracks. Here, the authors proposed a multifunction skin sensor that combines optical and electrical sensing properties. The optical function is passive and engineered to visually assist in localizing fatigue cracks, and the electrical function is added to send timely warnings to infrastructure operators. This is achieved by modifying the nanoscale structures within a photo-elastomer to obtain a soft stretchable optically-active film that is sandwiched between transparent carbon nanotube electrodes (CNT) to form a capacitor structure for adding electrical functionality. The developed sensor has a stiffness of 460 kPa and withstands reversible strain levels of up to 40%. Additionally, it exhibits a reversible and repeatable color change from light blue to deep blue, and changes the reflected color in the Vis spectra from approximately 500 nm to 600 nm and insensitive to viewing angle. The performance of the sensor is characterized through a free-standing dynamic test and further extended to a free-vibration test conducted on a steel cantilever plate. A correlation- based image processing algorithm was developed to discriminate color change and further quantify strain. The measured shift in the material's reflection center wavelength was merged with an RGB correlations matrix and an optical gauge factor of 0.52 was obtained. An electrical gauge factor of 0.48 was obtained by subjecting the sensor to a triangular load. It was found that the parallel capacitance measurements exhibited better performance by yielding higher accuracy for free vibration strain measurements.

Han Liu, Ph.D Student, Email: liuhan@iastate.edu. Department of Civil, Construction, and Environmental Engineering, Iowa State University, Ames, IA, 50011, USA
Matthias Kollosche, Researcher. Department of Civil, Construction, and Environmental Engineering

INTRODUCTION

Structural health monitoring (SHM) systems are technologies aimed at assisting or automating the condition assessment process of civil, mechanical, and aerospace infrastructures. Examples of traditional sensors used for SHM include optical fiber sensors [1, 2], resistive foil strain gauges [3, 4], accelerometers [5, 6], piezoelectric sensors [7, 8], linear variable differential transformers [9], and tiltmeters [10].

Recently, functionalized materials have been proposed to improve SHM performance by enabling distributed area- or volume-sensing. Examples include sensing skins [11,12] and self-sensing cementious composites [13, 14]. The vast majority of these solutions rely on electrical measurements and signal processing algorithms to notify infrastructure operators and/or inspectors of possible damage.

Others have proposed optical sensors to directly assist inspections through visual observations. Examples include microcapsule embedded coating [15], self-reporting mechanochromic composites [16], and fluorescence crack sensing [17,18]. The majority of these color-dynamic materials, such as the liquid crystalline elastomer, exhibit angle-dependent color changes that are difficult to apply in the field [19, 20]. To address this issue, elastically deformable fibers and photonic crystals have been doped into polymer to confer the structural color change property [21, 22]. Polymer-based nano-structurally colored materials that respond to external stimulus, such as mechanical strain, force, temperature, humidity, and light, with repeatable color changes or color emission have attracted significant attention in the SHM community due to their great potential for passive optical/visual sensing [23, 24].

The authors have recently proposed a multifunctional sensor technology that combines optical and electric signals for strain sensing [25]. The developed sensor comprises a flexible and stretchable structural color film sandwiched between two transparent carbon nanotube (CNT) electrodes to form a parallel plate capacitor structure. The technology was developed and demonstrated for the detection of fatigue cracks in steel. The structural color film is a photo-elastomer filled with silica nanoparticles (SiO_2) particles that acts as the photonic structure for density change, enabling a reversible, repeatable, and angle-independent color change under stretch. In this study, we extend work presented in [25] and characterise the optical and electric sensing properties under dynamic loads.

The rest of the paper is organized as follows. Section provides the background on the sensing technology, including the fabrication process and electromechanimal model. Section describes the experimental methodology. Section presents and discusses results from the experimental investigation. Section concludes the paper.

Iowa State University, Ames, IA, 50011, USA.
Simon Laflamme, Professor, Department of Civil, Construction, and Environmental Engineering, Iowa State University, Ames, IA, 50011, USA; Department of Electrical and Computer Engineering, Iowa State University, Ames, IA, 50011, USA
David R Clarke, Professor, Harvard John A. Paulson School of Engineering and Applied Sciences, Harvard University, Cambridge, MA, 02138, USA.

BACKGROUND

Fabrication

The multifunctional sensor is constituted by sandwiching a structural color film between CNT electrodes, and its design and fabrication process are described in detail in [25]. Briefly, the structural color film is fabricated by infilling 40 wt% silica particles (SiO_2) in the polymer matrix, which are produced by mixing poly(ethylene glycol) phenyl ether acrylate (PEGPEA, Sigma-Aldrich) with a photoinitiator (2-128 hydroxy-2-methyl-1-phenyl-1-propanone, Sigma-Aldrich) in a 1 w / w ratio. The silica particles, that have a diameter of 200 nm, are uniformly dispersed in the matrix using a shear mixer, and the resulting solution is drop-casted onto glass slides and cured under UV light and nitrogen atmosphere. The transparent electrodes are fabricated by diluting a commercially available CNT solution (Invision 3500, Nano-C) in isopropanol and vacuum filtered through a porous polytetrafluoroethylene (PTFE) membrane with a pore size of 0.5 μm. The resulting PTFE filter membrane has a sheet resistance of 600Ω Sq^{-}1 and is stamped onto both sides of the structural color film to form a capacitor structure. Two self-adhesive copper tabs are embedded in the electrodes to create electrical connections.

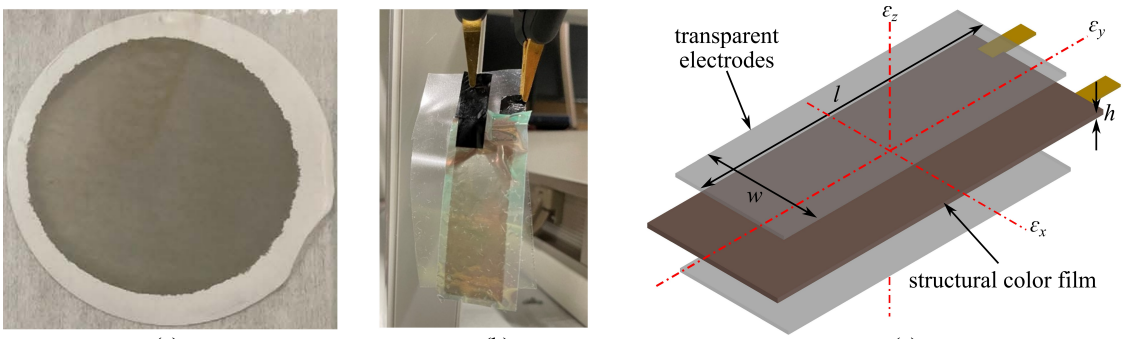

Figure 1. (a) Pictures of a PTFE filter membrane; (b) picture of the assembled sensor; and (c)annotated schematic of the corresponding sensor.

Electromechanical Model

At low measurement frequency ($< 1kHz$), the sensor can be modeled as a parallel capacitor for which the initial capacitance C_0 can be taken as:

$$C_0 = e_0 e_r \frac{A}{h} \tag{1}$$

where e_0 is the vacuum permittivity, e_r is the relative permittivity, A is the electrode area, and h is the thickness of the structural color film. The basic sensing principle for the sensor under an uniaxial strain (along the x-axis in Figure 1)) can be written as:

$$\frac{\Delta C}{C_0} = \frac{1}{1-\nu}(\varepsilon_x + \varepsilon_y) = \lambda_0(\varepsilon_x + \varepsilon_y) \tag{2}$$

where ΔC is the change in capacitance, ν is the Poisson's ratio of the structural color film, ε_x and ε_y are the in-plane strains, and λ_0 is the resulting gauge factor. In an adhered configuration, Eq. 2 becomes:

$$\frac{\Delta C}{C_0} = \frac{1-\nu_{xy}}{1-\nu}(\varepsilon_x) = \lambda \varepsilon_x \tag{3}$$

where ν_{xy} is the traversed Poisson's ratio of the sensor under composite action. The derivation of the electromechanical model is reported in [25].

Correlation Coefficient

To quantify strain measured from the optical color response, an image processing method was established by computing correlation coefficients J between two RGB color matrices that are produced from the color points in a defined region of interest (ROI), taken as:

$$\begin{aligned} J &= 1 - \frac{\mathbb{E}\left[(S_{i,k} - \mu_s)\right]\left[\left(S^0_{i,j} - \mu_{S^0}\right)\right]}{\sigma_s \sigma_{s^0}} \\ &= 1 - \frac{\sum_{i,k}\left(S_{i,k} - \mu_s\right)\left(S^0_{i,j} - \mu_{S^0}\right)}{\sqrt{\sum_{i=1}^{n}\left(S_{i,k} - \mu_s\right)^2}\sqrt{\sum_{i=1}^{n}\left(S^0_{i,j} - \mu_{S^0}\right)^2}} \end{aligned} \tag{4}$$

where $\mathbb{E}$ is the expectation, $S_{i,j}$ and $S^0_{i,j}$ are respectively the RGB matrices resulting from the first frame and the compared frame, μ_S and μ_{S^0} are respectively the means of $S_{i,j}$ and $S^0_{i,j}$ with their associated standard levitations and σ_s and σ_{s^0}. Details of the image processing method is reported in [25].

EXPERIMENTAL TEST

The optical and electrical sensing performance of the assembled sensor was characterized through a free-standing cyclic test, and the overall experimental setup is presented in Figure 2(a). Three independent specimens ($l \times w \times h$ = 56 × 8 × 0.15 mm^3) were prepared. Both ends of the sensor were gripped within the clamping fixtures mounted onto the loading cell of an Instron 5544A tensile tester. An LED light was used as the light source to provide the lighting level of an ambient environment, and a black plate was put behind the sensor to provide a high-resolution color contrast. A load of 0.05 N was pre-applied prior to each test to eliminate any slack in the sensor. A quasi-static test was conducted by applying uniaxial tensile strain along the longitudinal direction with a linear rate of 1% s^{-1} to achieve a strain target of 40% and then released at the same rate. This procedure was repeated five times. The dynamic test was conducted by subjecting specimens to a 0.1 Hz triangular cyclic loading with strain amplitude levels of 0.5, 1, 2, 3, and 4% each applied for five cycles, with the third cycle's maximum strain level maintained for a few seconds. Capacitance data were recorded by using an LCR meter (Keysight E4980A) at a sampling frequency of 100 Hz. A digital camera was placed in front of the specimen to simultaneously record the surface/apparent color of the sensor under different strain levels, and the frame rate was set to 60 fps.

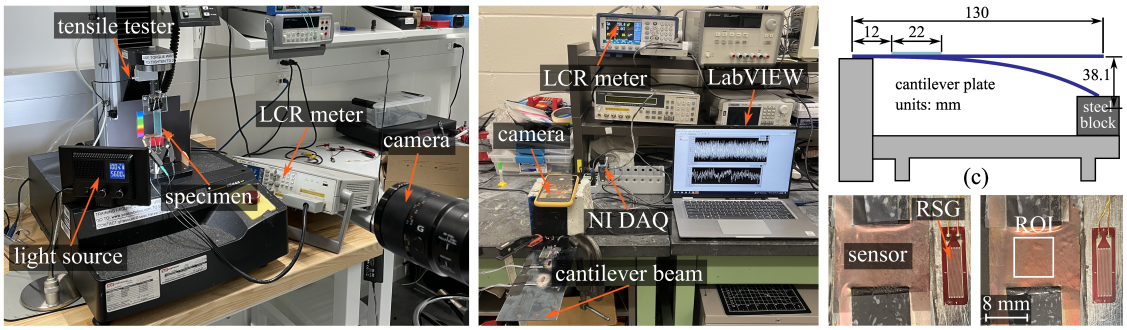

Figure 2. (a) Overall experimental setup of the free-standing tensile test; (b) experimental setup of the cantilever plate system; (c) schematic of the designed cantilever plate system (elevation view); (d) close up view of the sensor in the setup; and (e) digital photo showing the color of the sensor under the maximum tensile strain with the location of the ROI indicated.

The dynamic optical and electrical sensing performance of the sensor was further evaluated through free-vibration test conducted on a cantilever plate, as shown in Figure 2(b). The sensor was deployed on a steel plate of dimensions ($l \times w \times h$ = 252 x 103 x 0.8 mm^3) using a thin epoxy layer (JB-Weld), and an approximate 1% pre-strain was applied on the sensor to allow the measurement of compressive strain. A foil type resistive strain gauge (RGS) (TML FLA-10-350-11-1LJCT, SGC-28, nominal resistance of 350 $\pm$ 1.0 Ω, gauge length of 10 mm) was installed 3 mm away from the right-hand-side of the sensor using a non-conductive strain gauge adhesive (CN Cyanoacrylate) for benchmarking results (Figure 2(d)). For repeatability of the excitation, the free end of the cantilever was bent until in touched a steel block located 1.5 in (38.1 mm) below the tip (shown in Figure 2(c)), and free vibrations generated by releasing the free end. An LCR meter (BK Precision 891) was used to acquire capacitance data at a sampling frequency of 60 Hz, and a National Instrument three quarter bridge analog input modules (NI-9236) was used to collect the voltage output from the strain gauge at 1 kHz. A camera with a frame rate of 60 fps was placed at the top of the cantilever beam system to record the surface/apparent color of the sensor during vibrations. Figure 2(d) and (e) are pictures showing the sensor's color during a static position and under maximum tension strain, respectively. An 8 mm $\times$ 8 mm square-shape ROI was defined at the center of the sensor, identified by the white box in Figure 2(e), where 24 color points were uniformly assigned within to identify RGB values and form an RGB color matrix.

RESULTS AND DISCUSSION

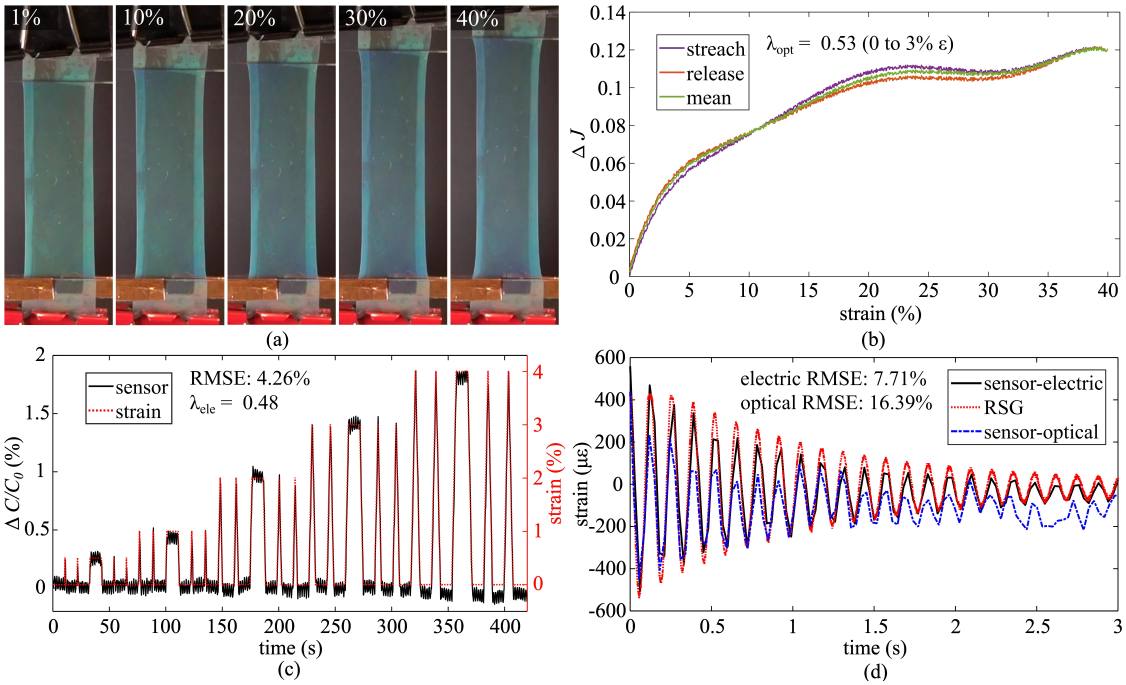

Figure 3. (a) Digital photos of the sensor at 1, 10, 20, 30, and 40% strain under ambient condition; (b) ΔJ as function of strain for the sensor during the stretch and release processes of the first 40% stain cycle; (c) time series plot of the sensor's capacitance response under triangular loading; and (d) comparison of the bending strain measured from the sensor and the RSG.

Figure 3(a) is the picture showing the sensor's apparent/surface color under 1, 10, 20, 30, and 40% strains, respectively, taken from the quasi-static test. Here, a strain-depended and naked-eye observable color change from emerald to deep blue was observed on the free-standing sensor under an ambient condition (normal white light).

Figure 3(b) presents a plot of change in correlation ΔJ as a function of strain produced from the stretch and release process of the quasi-static test, where the ΔJ was computed using Eq. 4. The green curve represents the mean value averaged from the measurements over 5 independent tests. An optical gauge factor λ_{opt} of 0.52 was established from over the region 0 to 4% strain.

Figure 3(c) plots the time series of the relative change in capacitance ($\Delta C/C_0$) under the applied triangular excitations The sensor yielded an electrical gauge factor λ_{ele} of 0.48 and a root mean square error (RMSE) of 4.26% between the capacitance signal and strain input. These results demonstrate the capability of the electrical function at strain tracking.

Figure 3(d) presents the time history plot of the raw data obtained from the free vibration test conducted on the cantilever steel plate. The sensor is found to be capable of tracking the bending strain measured from the RSG both optically and electrically. Here, the sensor's optical signal is obtained by processing the raw data with the optical gauge factor λ_{opt} of 0.53 characterized from prior tensile tests (Figure 3(b)), and similarly the electrical signal is processed using the electrical gauge factor λ_{ele} of 0.48 (Figure 3(c)). Images are processed with the BM3D image de-noising algorithm to filter noise caused

by the light source [26]. The electric function exhibited a better performance with an RMSE of 7.71% computed with respect to the measurements from RSG, compared with an RMSE of 16.39% for the optical function. The higher RMSE value for optical function can be attributed to the insufficient frame rate of the camera used in this study that can cause signal distortion through aliasing. Remark that the data collection of the optical signal can be improved by using a camera with a higher frame rate but also with the assistance of an optic spectrometer to measure reflected wavelength of the sensor's color.

CONCLUDING REMARKS

This paper presented a preliminary study characterizing the dynamic behavior of a multifunctional soft transducer that combines optical and electrical sensing functions. The optical function is passive and engineered to visually assist in localizing fatigue cracks, and the electrical function is added to send timely warnings to infrastructure operators. This is achieved by modifying the nanoscale structures within a photo-elastomer to obtain a soft stretchable optically-active film that is sandwiched between transparent carbon nanotube electrodes (CNT) to form a capacitor structure for adding electrical functionality.

The sensor was deployed on a cantilever plate to measure compressive and tensile bending strain produced under free-vibration, and results were compared against the measurement obtained from a commercial foil-type strain gauge. An optical gauge factor λ_{opt} of 0.52 and an electric gauge factor λ_{ele} of 0.48 were respectively obtained from a free-standing tensile test and a triangular load test, and used to process data from the free-vibration setup. Results show that both functions were capable of tracking free vibrations, with the electrical function over-performing the optical function, likely attributable to the frame rate of the camera. Furthermore, a higher optical strain sensitivity is expected with modifications of nanoparticle sizes and material and film processing. That modification will allow a larger wavelength tuning range and higher visual saturation of the color changes.

Overall, the present work showed the promise of the multifunctional sensor technology for in-situ SHM applications. Of interest, its optical function could be used for the detection of defects (e.g., fatigue crack) passively, without permanently installed electronics for data acquisition and transmission. It is expected that the developed sensor and computational methods can be applied beyond SHM, such as for human–computer interaction and soft robotics applications.

ACKNOWLEDGMENT

The authors gratefully acknowledge the financial support of the Departments of Transportation of Iowa, Kansas, South Carolina, and North Carolina, through the Transportation Pooled Fund Study TPF-5(449), and of the National Science Foundation through the Harvard University Materials Research Science and Engineering Center DMR-2011754.

REFERENCES

1. Das, S. and P. Saha. 2018. "A review of some advanced sensors used for health diagnosis of civil engineering structures," *Measurement*, 129:68–90, doi:10.1016/j.measurement.2018.07.008.
2. Wang, H., P. Xiang, and L. Jiang. 2019. "Strain transfer theory of industrialized optical fiber-based sensors in civil engineering: A review on measurement accuracy, design and calibration," *Sensors and Actuators A: Physical*, 285:414–426, doi:10.1016/j.sna.2018.11.019.
3. Liu, Z. and N. Mrad. 2013. "Validation of Strain Gauges for Structural Health Monitoring With Bayesian Belief Networks," *IEEE Sensors Journal*, 13(1):400–407, doi:10.1109/jsen.2012.2217954.
4. Hu, X., B. Wang, and H. Ji. 2012. "A Wireless Sensor Network-Based Structural Health Monitoring System for Highway Bridges," *Computer-Aided Civil and Infrastructure Engineering*, 28(3):193–209, doi:10.1111/j.1467-8667.2012.00781.x.
5. Garcia, D. and D. Tcherniak. 2019. "An experimental study on the data-driven structural health monitoring of large wind turbine blades using a single accelerometer and actuator," *Mechanical Systems and Signal Processing*, 127:102–119, doi:10.1016/j.ymssp.2019.02.062.
6. Ali, A., T. Sandhu, and M. Usman. 2019. "Ambient Vibration Testing of a Pedestrian Bridge Using Low-Cost Accelerometers for SHM Applications," *Smart Cities*, 2(1):20–30, doi:10.3390/smartcities2010002.
7. Giurgiutiu, V. 2007. "Structural health monitoring: with piezoelectric wafer active sensors," *Elsevier*.
8. Qing, X. P., S. J. Beard, A. Kumar, K. Sullivan, R. Aguilar, M. Merchant, and M. Taniguchi. 2008. "The performance of a piezoelectric-sensor-based SHM system under a combined cryogenic temperature and vibration environment," *Smart Materials and Structures*, 17(5):055010, doi:10.1088/0964-1726/17/5/055010.
9. Heininger, H., F. Mohr, U. Hannemann, and R. J. Schmidt. 2012. "Observation of prestress loss in post-tensioned concrete with FBG and LVDT sensors," in *2012 IEEE Conference on Prognostics and Health Management*, IEEE, doi:10.1109/icphm.2012.6299518.
10. Al-Qazweeni, J., J. Parol, H. A. Kamal, A. Al-Enezi, A. Bin-Nakhi, H. Sun, and O. Büyüköztürk. 2020. "Structural Health Monitoring System for Al-Hamra Tower in Kuwait City," in *Gulf Conference on Sustainable Built Environment*, Springer International Publishing, pp. 279–286, doi:10.1007/978-3-030-39734-0_17.
11. Yan, J., A. Downey, A. Cancelli, S. Laflamme, A. Chen, J. Li, and F. Ubertini. 2019. "Concrete Crack Detection and Monitoring Using a Capacitive Dense Sensor Array," *Sensors*, 19(8):1843, doi:10.3390/s19081843.
12. Aygun, L. E., V. Kumar, C. Weaver, M. Gerber, S. Wagner, N. Verma, B. Glisic, and J. C. Sturm. 2020. "Large-Area Resistive Strain Sensing Sheet for Structural Health Monitoring," *Sensors*, 20(5):1386, doi:10.3390/s20051386.
13. Abedi, M., R. Fangueiro, and A. G. Correia. 2021. "A review of intrinsic self-sensing cementitious composites and prospects for their application in transport infrastructures," *Construction and Building Materials*, 310:125139, doi:10.1016/j.conbuildmat.2021.125139.
14. Birgin, H. B., A. D'Alessandro, S. Laflamme, and F. Ubertini. 2021. "Innovative Carbon-Doped Composite Pavements with Sensing Capability and Low Environmental Impact for Multifunctional Infrastructures," *Journal of Composites Science*, 5(7):192, doi:10.3390/jcs5070192.
15. Zheng, X., Q. Wang, Y. Li, J. Luan, and N. Wang. 2019. "Microcapsule-Based Visualization

Smart Sensors for Damage Detection: Principles and Applications," *Advanced Materials Technologies*, 5(2):1900832, doi:10.1002/admt.201900832.

16. Tabatabaeian, A., S. Liu, P. Harrison, E. Schlangen, and M. Fotouhi. 2022. "A review on self-reporting mechanochromic composites: An emerging technology for structural health monitoring," *Composites Part A: Applied Science and Manufacturing*, 163:107236, doi:10.1016/j.compositesa.2022.107236.
17. Song, Y.-K., K.-H. Lee, W.-S. Hong, S.-Y. Cho, H.-C. Yu, and C.-M. Chung. 2012. "Fluorescence sensing of microcracks based on cycloreversion of a dimeric anthracene moiety," *J. Mater. Chem.*, 22(4):1380–1386, doi:10.1039/c1jm13709c.
18. Song, Y. K., B. Kim, T. H. Lee, S. Y. Kim, J. C. Kim, S. M. Noh, and Y. I. Park. 2018. "Monitoring Fluorescence Colors to Separately Identify Cracks and Healed Cracks in Microcapsule-containing Self-healing Coating," *Sensors and Actuators B: Chemical*, 257:1001–1008, doi:10.1016/j.snb.2017.11.019.
19. Phillips, K. R., G. T. England, S. Sunny, E. Shirman, T. Shirman, N. Vogel, and J. Aizenberg. 2016. "A colloidoscope of colloid-based porous materials and their uses," *Chemical Society Reviews*, 45(2):281–322, doi:10.1039/c5cs00533g.
20. Kim, S.-U., Y.-J. Lee, J. Liu, D. S. Kim, H. Wang, and S. Yang. 2021. "Broadband and pixelated camouflage in inflating chiral nematic liquid crystalline elastomers," *Nature Materials*, 21(1):41–46, doi:10.1038/s41563-021-01075-3.
21. Fudouzi, H. and T. Sawada. 2005. "Photonic Rubber Sheets with Tunable Color by Elastic Deformation," *Langmuir*, 22(3):1365–1368, doi:10.1021/la0521037.
22. Arsenault, A. C., T. J. Clark, G. von Freymann, L. Cademartiri, R. Sapienza, J. Bertolotti, E. Vekris, S. Wong, V. Kitaev, I. Manners, R. Z. Wang, S. John, D. Wiersma, and G. A. Ozin. 2006. "From colour fingerprinting to the control of photoluminescence in elastic photonic crystals," *Nature Materials*, 5(3):179–184, doi:10.1038/nmat1588.
23. Zeng, S., D. Zhang, W. Huang, Z. Wang, S. G. Freire, X. Yu, A. T. Smith, E. Y. Huang, H. Nguon, and L. Sun. 2016. "Bio-inspired sensitive and reversible mechanochromisms via strain-dependent cracks and folds," *Nature Communications*, 7(1), doi:10.1038/ncomms11802.
24. Pulliam, E., G. Hoover, and D. Ryu. 2017. "Multifunctional Mechano-Luminescent-Optoelectronic Composites for Self-Powered Strain Sensing," in *Volume 2: Modeling, Simulation and Control of Adaptive Systems Integrated System Design and Implementation Structural Health Monitoring*, American Society of Mechanical Engineers, doi:10.1115/smasis2017-3977.
25. Liu, H., M. Kollosche, S. Laflamme, and D. R. Clarke. 2023. "Multifunctional Soft Stretchable Strain Sensor for Complementary Optical and Electrical Sensing of Fatigue Cracks," *Smart Materials and Structures*.
26. Yahya, A. A., J. Tan, B. Su, M. Hu, Y. Wang, K. Liu, and A. N. Hadi. 2020. "BM3D image denoising algorithm based on an adaptive filtering," *Multimedia Tools and Applications*, 79(27-28):20391–20427, doi:10.1007/s11042-020-08815-8.